

# KAN-Mamba FusionNet: Redefining Medical Image Segmentation with Non-Linear Modeling

Akansh Agrawal\*  
akanshcs2020@gmail.com

Akshan Agrawal\*  
akshanacs2020@gmail.com

Shashwat Gupta  
guptashashwatme@gmail.com

Priyanka Bagade†  
pbagade@iitk.ac.in  
Indian Institute of Technology Kanpur  
Kanpur, Uttar Pradesh, India

## Abstract

*Medical image segmentation is crucial in robotic surgeries, disease diagnosis, and treatment plans. This research presents an innovative methodology that combines Kolmogorov-Arnold Networks (KAN) with an adapted Mamba layer for medical image segmentation. The proposed KAN-Mamba FusionNet framework improves image segmentation by integrating attention-driven mechanisms with convolutional parallel training and autoregressive deployment, while preserving interpretability, in contrast to the state-of-the-art techniques that depend exclusively on Mamba for ailment localization and accurate diagnosis. We evaluated our proposed KAN-Mamba FusionNet model on three distinct medical image segmentation datasets, BUSI, Kvasir-Seg and GlaS. The results indicated that the KAN-Mamba FusionNet consistently yields better IoU and F1 scores in comparison to the state-of-the-art methods. Further, we offer insights into the model's behavior via ablation studies, examining the effects of various components and assessing their contributions to the overall performance of the proposed model. The findings illustrate the strength and effectiveness of this methodology for dependable medical image segmentation, providing a unique approach to address intricate visual data issues in healthcare.*

## 1. Introduction

Medical image segmentation can help with the accurate localization of anatomical features, leading to the timely detection of abnormalities and patient treatment. Recent research into developing advanced deep learning and computer vision-based approaches has provided a gateway to

address the challenges faced in the localization of diseased organs [6, 16, 27, 35]. Reliable image segmentation techniques are vital for helping medical experts make informed decisions and improve diagnosis outcomes. This can potentially increase the life expectancy of the patients.

Convolutional Neural Networks (CNNs) are popularly used to mark individual pixels for segmentation tasks to identify tumor locations, organs, and relevant anatomical features. Classical CNN-based approaches like UNet models [27] are based on encoder and decoder architecture for image segmentation. The UNet variations, UNet [27], UNet++ [36], and UNet3+ [13] use skip connections to combine the related low-level detailed feature maps from the encoder and the high-level semantic feature maps from the decoder. Since these models use hierarchical techniques to extract features from the input image, they fail to get global contextual dependencies, which are essential to segment varied-sized anatomical parts from the medical image.

Unlike CNNs, ViT i.e. vision transformers [7] use attention mechanism to capture the global contextual dependencies and can accept varied input sizes, making them better suitable for the medical image segmentation task [5]. However, transformers suffer from large model sizes, high memory, and computational requirements due to long-run feature extractions.

In order to overcome the challenges of higher computational complexity of transformers, state space models (SSM) using linear RNNs (Recurrent Neural Networks) are proposed as Mamba architecture [9]. Different variants of Mamba architecture, such as U-Mamba [23], Vision Mamba [32], and SegMamba [33] were introduced to improve the overall efficiency of the medical image segmentation by employing selective state representations that dynamically adjust based on the input data. These models were able to achieve the time complexity of  $O(n \log(n))$  which is much lower than the transformers.

\* The first two co-authors are both designated as first authors and contributed equally. † Corresponding author

The Mamba-based models use the convolution layers which are similar to Multi-Layer Perceptrons (MLPs). In past, the MLP layers have been replaced with KAN Architecture [22] to capture the nonlinear intricacies in the images. For instance, the boundaries between the features of images may not capture a linear relation, leading to a loss of some important details from the medical images which can potentially result in incorrect disease diagnosis. To address this issue the U-KAN based approach was proposed for medical image segmentation [18] by learning the activation functions to capture the non-linear features. However, the approach utilized in KAN-based architecture has a disadvantage over Mamba because of its inability to capture self-attentive based learning over intricate spatial features from the images [34].

In this paper, we propose KAN-Mamba FusionNet model for medical image segmentation to address the challenges posed by the currently available techniques. The proposed architecture incorporates KAN in Mamba layer and enables the integration of non-linear transformations to improve the representation of complex medical imaging data. Here, we leverage the synergy of KAN and Mamba-based architectures to overcome the limitations of conventional CNNs and Transformers, particularly in their ability to capture long-range dependencies and handle image segmentation datasets efficiently.

Moreover, standard activation functions such as ReLU, sigmoid, and tanh used in the MLPs, Mamba and KAN models possess distinct advantages and drawbacks. For example, ReLU provides efficiency and sparsity but may encounter the "dying ReLU" issue, whereas sigmoid and tanh are suitable for probability modeling but are susceptible to vanishing gradients. To tackle these issues, we present the Bag-of-Activation (BoA) Functions in our proposed approach, which integrates many activation functions via a weighted sum with adjustable parameters. This approach enables neural networks to flexibly leverage the benefits of various activation functions, hence augmenting their capacity to represent intricate data patterns and enhancing overall efficacy.

Here is the summary of our contributions:

- We propose a novel neural network architecture, KAN-Mamba FusionNet, that incorporates Mamba block in the U-KAN model to introduce self-attention layers for complex contextual understanding from the input data for improved localization.
- We additionally introduce an innovative enhancement by adding another KAN layer within the Mamba architecture to further integrate learning over any non-linear intricacies in the input.
- Further, we introduce the support of Bag of Activation (BoA) functions in the Mamba block, which dynamically combines multiple activation functions to provide a more

robust representation of features.

- We evaluated our proposed architecture on medical image datasets, BUSI [1], GlaS [29] and Kvasir-Seg [14] and provided ablation study in the end.

## 2. Related Work

Medical image segmentation is crucial for enabling accurate diagnosis and treatment planning. Architectures like U-Net, characterized by its encoder-decoder structure, have shown significant success in this domain [27]. Extensions such as Unet++ [36] and CE-Net [10] incorporate sophisticated modules for multi-scale feature fusion and contextual encoding to improve segmentation accuracy. In addition to convolution-based approaches, transformer models [31] like Vision Transformer [8], Medical Transformer [30], and TransUNet [5] have been applied, using attention mechanisms to capture long-range dependencies. Methods like 3D segmentation [15] and multi-dimensional gated recurrent units [2] have shown promise in tasks requiring volumetric understanding. Recently, Mamba-based architectures have emerged, utilizing state-space models (SSMs) for fast linear-time inference and cross-scan modules [9, 20]. Their applications, especially on biomedical image segmentation datasets, highlight their growing importance in medical imaging.

Kolmogorov-Arnold Networks (KANs) offer an innovative alternative to traditional MLPs for medical segmentation. Based on the Kolmogorov-Arnold theorem, KANs efficiently approximate multivariate continuous functions using univariate transformations, enabling the capture of nonlinearities in high-dimensional data [12]. KANs are distinguished by their interpretability, robustness, and efficiency, making them suitable for applications requiring precision, such as medical imaging. While their application in medical segmentation is nascent, models like U-KAN that employ learnable weights and nonlinear transformations have shown potential for extracting insights from various medical datasets.

Mamba-based models are designed to address the limitations of convolutional neural networks (CNNs) in capturing long-range dependencies. Vision Mamba (Vim) and VMamba have demonstrated improved effectiveness in video understanding and remote sensing tasks by combining state-space models with attention mechanisms [20]. In medical imaging, these models have proven particularly efficient in segmentation, utilizing approaches such as transfer learning on biomedical image segmentation datasets. A comparative study of these architectures with CNNs and Vision Transformers (ViTs) has highlighted the trade-offs in terms of data requirements, interpretability, and performance.

Biomedical image segmentations has seen several algorithmic improvements. Hybrid models such as the Hybrid

Adaptive Attention Module (HAAM)-based U-Net [4] and attention-guided U-Net [26] have achieved high precision and accuracy, using attention mechanisms to enhance feature extraction. Alternative designs like U2-MNet [19] and SU-Next [37] employ advancements such as residual inception depth-wise separable convolution and multilayer perceptron frameworks to improve segmentation speed and accuracy. Models like the Feature Pyramid Non-Local Network [28] and cascaded CNNs [3] have improved performance metrics on datasets like Breast UltraSound Images (BUSI), achieving significant dice scores. Techniques such as transfer learning and novel attention mechanisms are advancing image segmentation, with KANs and Mamba-based models offering viable alternatives to traditional CNN structures.

In this paper, we propose a novel architecture, KAN-Mamba FusionNet, which leverages the non-linear intricacies captured by KAN as well as utilizes the capabilities of Mamba to capture the implicit spatial features from the input images.

### 3. Proposed Architecture

The proposed KAN-Mamba FusionNet architecture integrates the attentive-driven mechanism with the robust KAN non-linear model [12]. The idea is to replace the convolution and batch normalization layers (which are similar to MLPs) used before the SSM model in the traditional Mamba [9] with the KAN block. Figure 1 represents the overall architectural flow of our proposed model. It utilizes the U-KAN architecture [18] as a base. The notations or color encoding done in the overall architecture diagram (Figure 1) represent the following:

- **C1/C2/C3**: Represents the convolution block ( $ConvB$ ).
- **P1/P2**: Represents the patch embedding layer.
- **M1**: Represents the modified Mamba-KAN block.
- **L1/L2**: Represents the layer normalization.
- **D1/D2/D3/D4/D5**: Represents the DepthWise Convolution ( $DwConvB$ ) Block.
- **K1/K2/K3/K4**: Represents the KAN Block.
- **O1**: Represents Conv2D layer, yielding the final output.

The proposed architectural flow is inspired by the KAN blocks used in the past in the replacement of the traditional MLP layer [12]. To capture the non-linear intricacies, KAN use learnable weights over edges. Similarly, in the past there has been usage of SSM and attentive layer to selectively process the input given and extract the relevant information [20]. Combining those, we propose to use a Mamba block with the KAN block. Further, since Mamba blocks consist of the convolution and batch norm layers (which is similar to the processing method of traditional MLP), we propose a change to replace those layers with a single KAN

layer. Moreover, we propose an idea to use a variation in activation function by replacing a single activation function with a bag of activation functions, where the model learns the weights assigned to each of the functions. The implementation of the proposed architecture blocks is explained in detail as follows:

**Convolutional Block**: The Convolution blocks C1/C2/C3, as shown in Figure 2, consist of 2D convolution layers, batch normalization layers, a max pooling layer and ReLU activation functions.

Let us represent this block transformation as  $ConvB(\cdot)$  such that :

$$Z_{out} = ConvB(Z_{in}) \quad (1)$$

where  $Z_{in}$  is the input sent to the convolution block.

In a similar way, as depicted in Figure 3, we have expressed depthwise convolution block,  $DwConvB$  by replacing pool operation in  $ConvB$  by interpolation operation:

$$Z_{out} = DwConvB(Z_{in}) \quad (2)$$

**Mamba Block**: The Mamba block is added after the first convolutional block,  $ConvBC1$  as shown in Figure 1. The input data passes through the linear projection layer while keeping the original input intact for the final linear combination. After the linear projection, the convolution kernel layer is applied, convolving over the 2D spatial dimensions. Further, it is processed via batch normalization 2D layer and a spatial attention layer. The step from convolution to batch normalization is organized into a series, forming a three-mini-block structure, with a spatial attention layer separating these blocks. The output is then passed through the activation function, which is further fed into a State Space Model (SSM) block. Additionally, a spatial attention layer is applied for the final processing.

The attentive layer on the Convolutional Block Attention Module can be expressed as [34]:

$$\begin{aligned} M_s(F) &= \sigma(f_{7 \times 7}([\text{AvgPool}(F); \text{MaxPool}(F)])) \\ &= \sigma(f_{7 \times 7}([F_{savg}; F_{smax}])) \end{aligned} \quad (3)$$

here,  $\sigma$  represents the sigmoid function acting over a larger convolution function  $f_{7 \times 7}$  having filter size of  $7 \times 7$  to capture more spatial features.

After reshaping, this output is linearly combined with the input (forming a skip connection) and with the output of the activation function in which the same input was fed.

**Bag of Activation Functions**: The single activation function,  $\text{sulu}$ , utilized in the Mamba block is substituted with the bag of activation functions. The model learns the weights assigned to the bag of activation functions to find

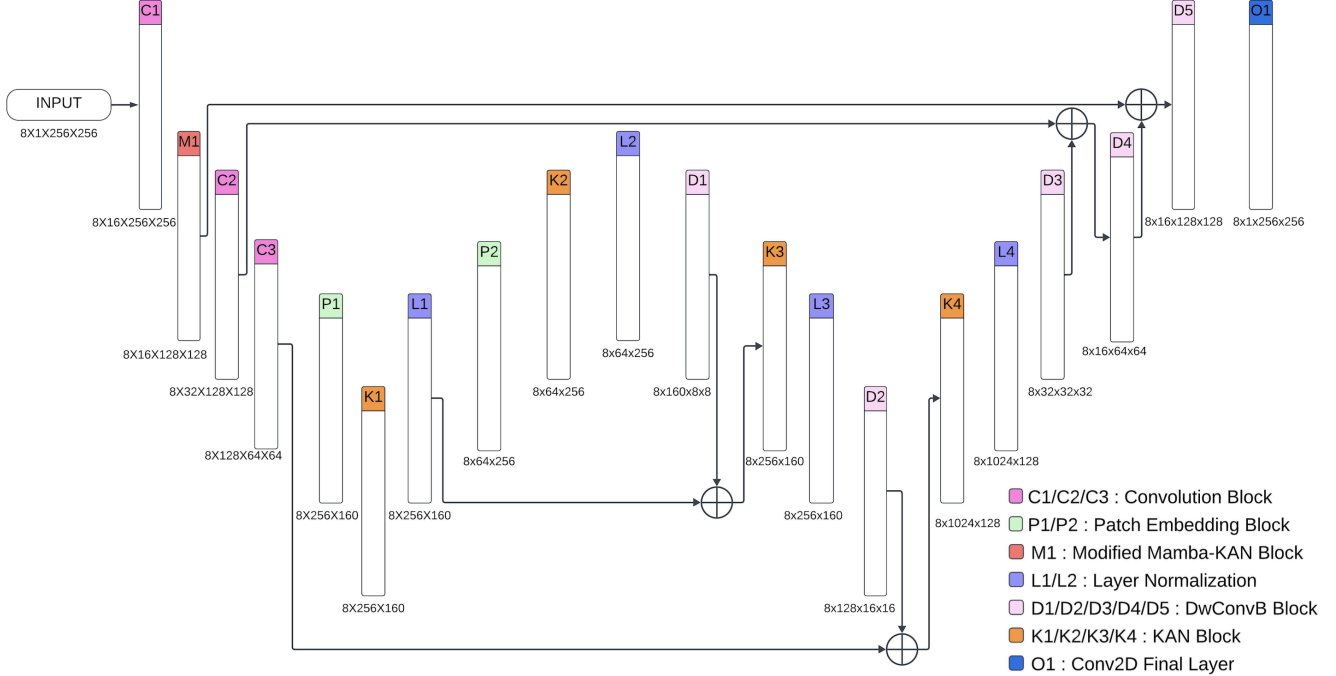


Figure 1. Overall Architectural Diagram. Note that each layer is connected with the next adjacent layer along with other explicit connections mentioned.

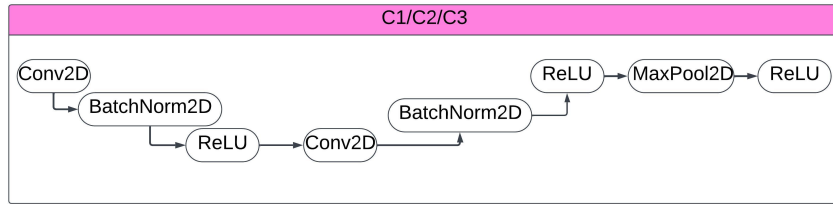


Figure 2. Convolution Block (*ConvB*)

the most effective function.

The bag of activation function can be expressed as :

$$\Psi(Z) = \sum_{p=1}^P \alpha_p \psi_p(Z) \quad (4)$$

where  $\alpha_p$  forms the learnable weight associated with activation function  $\psi_p$ . In our architecture, we have included following activation functions in the bag - ReLU, Tanh, Softplus, GELU and SiLU, keeping same initial weights.

**KAN in Mamba:** As shown in Figure 4, the architecture of this block primarily differs in the convolution layers used in Mamba before the SSM. Those convolution layers are replaced with a KAN block [18]. The input data is first passed through a patch embedding layer and then processed with a single KAN layer. Further, the output is passed through an

activation function, which is then fed into an SSM block. After spatial transformation, the results are processed by a spatial attention layer, followed by a linear projection layer. The resizing done in the projection layer helps to linearly combine the output with the input (from skip connection) and the output of the activation layer on the same input.

The MLP having K layers can be expressed in following form [18]:

$$\text{MLP}(Z) = (W_{K-1} \circ \sigma \circ W_{K-2} \circ \sigma \circ \dots \circ W_1 \circ \sigma \circ W_0) Z \quad (5)$$

where  $W_k$  with  $k \in [1, K]$  represent the transformation matrix,  $\sigma$  is the activation function and  $Z$  is the input data.

In a similar way we can write KAN formulation [18]:

$$\text{KAN}(Z) = (\Phi_{K-1} \circ \Phi_{K-2} \circ \dots \circ \Phi_1 \circ \Phi_0) Z \quad (6)$$

where  $\Phi$  are expressed using learnable activation functions

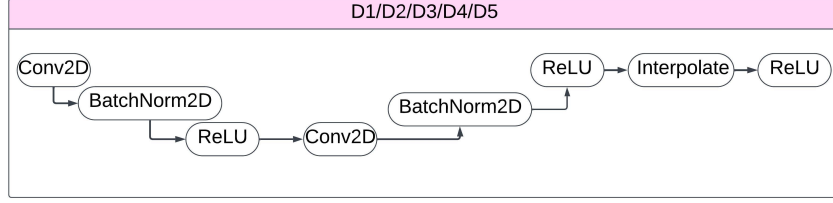


Figure 3. Depth-Wise Convolution Block ( $DwConvB$ )

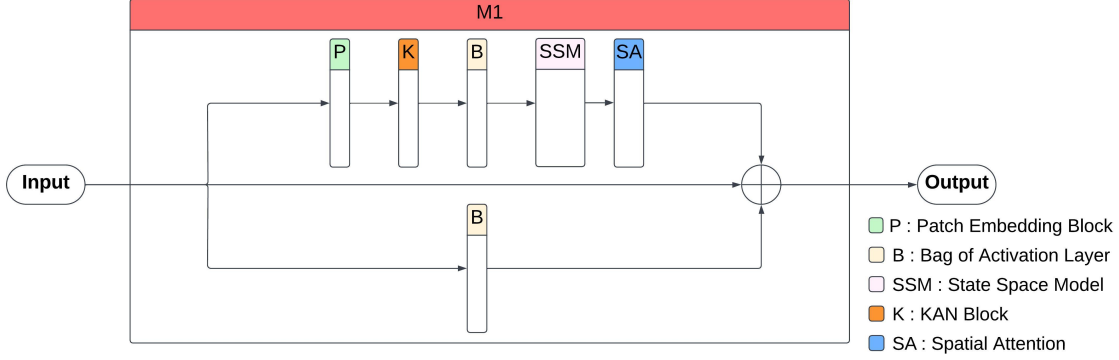


Figure 4. Modified Mamba-KAN Block

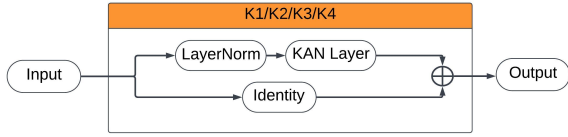


Figure 5. KAN Block

$\phi$  such that

$$\Phi = \{\phi_{q,p}\}, \quad p = 1, 2, \dots, n_{in}, \quad q = 1, 2, \dots, n_{out} \quad (7)$$

The KAN layer consists of the KAN Linear transformation [18], followed by a depthwise convolution  $DwConv$  layer (which consists of Conv2D Layer, followed by a batch normalization and a ReLU activation function). The basic unit of KAN layer can be represented as:

$$Z_{out} = (DwConv \circ KANLinear)Z_{in} \quad (8)$$

Such transformation is repeated thrice to get the KAN layer.  $KANB(\cdot)$  is used for denoting the KAN block comprising of a KAN layer, a normalization layer, and an identity function as shown in Figure 5.

Therefore, output can be mathematically denoted as:

$$\Gamma_{out} = KANB(Z_{in}) \quad (9)$$

where  $Z_{in}$  is the input passed through the KAN block.

Now, the mathematical formulation of modified Mamba-KAN block is explained below in detail.

The input  $Z_{in}$  is first passed through a patch embedding layer.

$$Z_{out} = PatchEmbed(Z_{in}) \quad (10)$$

The  $PatchEmbed(\cdot)$  represents the similar tokenization step in Tokenized KAN phrase operation as proposed in Seg. U-KAN model [18]. Then this is fed into KAN block such that :

$$Z'_{out} = KANB(Z_{out}) \quad (11)$$

where the  $KANB(\cdot)$  operation as mentioned earlier represent the KAN block transformation. This is further processed by a layer of Bag of Activation (BoA) Functions such that

$$Z''_{out} = \Psi(Z'_{out}) \quad (12)$$

Further, the output is passed through state space model (SSM) for transformation to get the following output:

$$Z'''_{out} = SSM(Z''_{out}) \quad (13)$$

After this, an attentive layer is added, which results in the following:

$$Z''''_{out} = M_s(Z'''_{out}) \quad (14)$$

where  $M_s(\cdot)$  represents the attentive function as explained above already.

Finally, combination with the skip connection and a parallel layer of BoA Functions gives final output as

$$\Omega_{\text{out}}(Z_{\text{in}}) = Z_{\text{out}}''' \oplus Z_{\text{in}} \oplus \Psi(Z_{\text{in}}) \quad (15)$$

Moreover, the loss for overall architecture is calculated using a combination of binary cross entropy (BCE) loss function and dice loss function, measuring the deviation from ground truth labels for entire set of N pixels.

$$\text{BCE}(\hat{z}, z) = -\frac{1}{N} \sum_{i=1}^N (z_i \cdot \log(\hat{z}_i) + (1 - z_i) \cdot \log(1 - \hat{z}_i)) \quad (16)$$

$$\text{DiceLoss}(\hat{z}, z) = 1 - \frac{2 \sum_{i=1}^N \hat{z}_i \cdot z_i + c}{\sum_{i=1}^N \hat{z}_i + \sum_{i=1}^N z_i + c} \quad (17)$$

where  $z_i$  and  $\hat{z}_i$  represent the pixel-wise label from actual and estimated measures respectively. A small constant  $c$  is included in dice loss to handle division by zero.

## 4. Datasets

We evaluated our model on three distinct medical image segmentation datasets: Breast UltraSound Images (BUSI) [1], Segmented Polyp Images [14] and Gland Segmentation Images (GlaS) [29]. Given the unique characteristics of each dataset, these evaluations offer a strong support for testing the effectiveness of our method.

**BUSI** [1]: The dataset consists of medical images from ultrasound scans, along with their corresponding segmentation masks, used for identifying breast cancer-related tumors. The entire set consists of 708 images, out of which 210, 437 and 133 represent the respective number of images for malignant, benign and normal breast cancer cases. We utilized the images representing breast cancer. The images were uniformly resized to  $256 \times 256$  pixels.

**Kvasir-Seg** [14]: Kvasir-SEG dataset consists of 1000 gastrointestinal polyp images (polyps are precursors to colorectal cancer) and their corresponding segmentation masks, which were manually annotated by a medical doctor and subsequently verified by an experienced gastroenterologist. All images were uniformly resized to  $256 \times 256$  pixels.

**GlaS** [29]: The dataset consists of gland segmentation images and is associated with the Hospital Clinic in Barcelona, Spain. For our study, we used 165 images from the dataset, all resized to  $256 \times 256$  pixels.

## 5. Experiments and Results

### 5.1. Implementation Details

For all three datasets, we set the learning rate to  $1e-4$  and trained with the Adam optimizer, incorporating a cosine annealing learning rate scheduler with a minimum learning

rate of  $1e-5$ . The loss function used was a combination of binary cross-entropy and dice loss. Each dataset was split in a 4:1 ratio for training and validation, respectively. Training was conducted over 400 epochs, with basic data augmentations like random rotation and flipping, applied to the inputs.

### 5.2. Evaluation Details

To evaluate the model’s performance, we reported validation IoU (Intersection over Union) and F1 Score on all the datasets and compared with the state-of-art methods. The IoU measures the overlap between predicted and ground truth segments, while the F1 score provides a balanced measure of precision and recall. These metrics are crucial for understanding the model’s accuracy and reliability across various segmentation tasks. The reported results are averages from three independent runs. We also present computational cost metrics such as GFLOPs and the total number of model parameters, and compare these with state-of-the-art methods. Additionally, we performed an ablation studies of our model, with the help of other useful parameters.

### 5.3. Performance Comparisons With State-of-Art Methods

Table 1 shows performance comparisons with other state-of-art methods on image segmentation on the three datasets. We introduce comparisons to the five state-of-art methods, U-Net [27], U-NeXt [30], Rolling-UNet [21], U-Mamba [24], and Seg. U-KAN [18]. Our experimental results demonstrate that, across all datasets, our proposed method, KAN-Mamba FusionNet, consistently performs well in comparison to other state-of-the-art approaches.

Our model performance, as demonstrated in terms of both metrics, IoU and F1 score, clearly indicates its robustness and versatility in handling diverse segmentation challenges. Further, as F1 score provides a balanced measure of precision and recall, in medical diagnosis, this model is very effective at identifying the actual positive cases, minimizing the number of false negatives (i.e., failing to detect cases where the condition is actually present), as such a failure in detection could be dangerous, leading to serious consequences for anyone.

Additionally, as shown in Table 2 we have calculated the GFLOPs and model parameters to emphasize that our model can be implemented with minimal trade-off in computational cost in contrast to previous methods.

### 5.4. Ablation Studies

We do a comprehensive evaluation of our proposed KAN-Mamba FusionNet under various settings, specifically to understand the effect of some added features in our model.

**Effect of Changes in Mamba Block:** Table 3 shows the results of the ablation study to validate the effect of

Method	BUSI [1]		Kvasir-Seg [14]		GlaS [29]	
	IoU↑	F1↑	IoU↑	F1↑	IoU↑	F1↑
U-Net [27]	56.43 ± 0.47	72.17 ± 0.02	72.41 ± 0.37	83.43 ± 1.12	82.18 ± 0.47	90.17 ± 0.48
U-NeXt [30]	58.21 ± 0.40	73.15 ± 0.32	69.36 ± 0.26	81.50 ± 0.14	82.54 ± 0.61	90.12 ± 0.21
Rolling-UNet [21]	59.85 ± 0.04	74.47 ± 0.02	75.51 ± 1.07	85.71 ± 0.42	83.25 ± 0.81	90.50 ± 0.82
U-Mamba [24]	59.05 ± 0.41	73.74 ± 0.12	73.91 ± 0.61	85.23 ± 0.52	84.42 ± 0.56	91.45 ± 0.32
Seg. U-KAN [18]	59.23±1.87	73.79±1.48	75.85 ± 0.53	85.96 ± 0.35	84.75 ± 0.32	91.70 ± 0.20
KAN-Mamba FusionNet	62.41±0.65	76.41±0.56	76.95 ± 0.68	86.66 ± 0.43	84.92 ± 0.45	91.82 ± 0.27

Table 1. Performance comparison of various segmentation methods on BUSI, Kvasir-Seg and GlaS datasets.

Method	Complexity	
	GFLOPS	Params (M)
U-Net [27]	524.2	34.53
U-NeXt [30]	3.98	1.47
Rolling-UNet [21]	13.41	1.78
U-Mamba [24]	2087	86.3
Seg. U-KAN [18]	13.87	6.36
KAN-Mamba FusionNet	13.96	6.37

Table 2. Model complexity comparison of various methods.

modifications in the Mamba block. As shown in Table 3, the Mamba + MLP combination represents the classical Mamba followed by an MLP layer. However, the classical model underperforms, whereas replacing the MLP layer with KAN layers leads to improvements in IoU, F1, accuracy, AUC, precision as well as recall, as indicated by the validation metrics in the table. Furthermore, incorporating a bag of activation functions alongside in classical Mamba, and then replacing the MLP layer with KAN layers (as proposed in our model), further improves the listed performance parameters.

**Effect of Bag of Activation Functions:** As shown in Table 4, the model initially performed sub-optimally when no additional activation function layer is added to the Mamba block, as proposed in our architecture. However, when a single activation function (say, ReLU) is introduced, the model’s performance improved significantly. Furthermore, by incorporating a composition of multiple activation functions, essentially a ”Bag of Activation functions”, the model’s learning capability is further enhanced, leading to even better results. These results underscore the importance of adding a bag of activation functions, demonstrating that the diversity of activation functions plays a important role in enhancing the performance of the model.

Different activation functions capture distinct aspects of data, each bringing their own strengths and weaknesses to a neural network. For instance, the Rectified Linear Unit (ReLU) [25] is defined as:

$$\text{ReLU}(x) = \max(0, x) \quad (18)$$

ReLU introduces sparsity by activating only for positive

inputs, which can lead to faster convergence and reduced computational complexity. However, ReLU can suffer from the “dying ReLU” problem, where neurons may become inactive and stop learning if they consistently output zero. On the other hand, the sigmoid function [11], defined as:

$$\sigma(x) = \frac{1}{1 + e^{-x}}, \quad (19)$$

is adept at modeling probabilities and is useful in scenarios requiring output values between 0 and 1. Nonetheless, it is prone to vanishing gradients, which can hinder the training of deep networks. Similarly, the hyperbolic tangent (tanh) [17] activation function:

$$\tanh(x) = \frac{e^x - e^{-x}}{e^x + e^{-x}}, \quad (20)$$

captures symmetric relationships around zero, providing outputs in the range of -1 to 1, which can help in centering the data and improving convergence. Yet, it also suffers from vanishing gradient issues.

To address these limitations, we proposed a combining multiple activation functions into a Bag of Activation (BoA) Functions as defined in the equation (4). This formulation allows the network to explore a richer function space, enhancing its ability to model diverse patterns in the data. By optimizing the weights associated with each activation function during training, the model can leverage the strengths of each activation function while mitigating their individual weaknesses.

For example, the combination can dynamically balance the sparsity introduced by ReLU with the probabilistic modeling of sigmoid and the zero-centered outputs of tanh. This adaptive weighting is achieved through gradient-based optimization, ensuring that the network selects the most appropriate activation behavior for different tasks or data characteristics.

Furthermore, different parts of the network might benefit from different activation behaviors, enabling more specialized and adaptive nonlinear transformations. By enabling the network to adaptively combine multiple activation functions, the Bag of Activation Functions approach offers a robust and versatile mechanism for enhancing neural network performance in diverse machine learning tasks.

Blocks and/or Layers	Performance Metrics					
	IoU $\uparrow$	F1 $\uparrow$	Accuracy $\uparrow$	AUC $\uparrow$	Precision $\uparrow$	Recall $\uparrow$
Mamba + MLP	58.81	73.27	92.53	91.96	74.43	72.58
Mamba + KAN	60.64	74.98	92.93	92.70	75.18	75.07
Mamba with BoA + KAN	61.35	75.40	93.26	92.78	76.68	73.48
KAN-Mamba FusionNet	62.41	76.41	93.42	93.33	77.76	75.41

Table 3. Ablation studies on the effect of introducing changes in the Mamba block on the model on BUSI dataset.

Activation Functions	Performance Metrics					
	IoU $\uparrow$	F1 $\uparrow$	Accuracy $\uparrow$	AUC $\uparrow$	Precision $\uparrow$	Recall $\uparrow$
None	60.64	74.98	92.93	92.70	75.18	75.07
Single (ReLU)	61.73	75.92	93.28	93.24	77.49	74.91
Proposed BoA	62.41	76.41	93.42	93.33	77.76	75.41

Table 4. Ablation studies on the effect of bag of activation in Mamba block of the model on BUSI dataset.

## 6. Conclusion

In this paper, we propose KAN-Mamba FusionNet architecture for medical image segmentation. It integrates Kolmogorov-Arnold Networks (KAN) with Mamba, and the bag of activation functions to reduce complexity, capture non-linearity in the input images, and adaptively select the efficient activation function to boost the model performance respectively. Our experiments across BUSI, Kvasir-Seg and Glas datasets validate our hypothesis, demonstrating better IoU (Intersection over Union) and F1 (Dice) scores on comparison with the SOTA methods. Furthermore, ablation studies show the key role of each architectural component, particularly highlighting how the bag of activation functions contributes to the overall performance enhancements. In summary, KAN-Mamba FusionNet advances accuracy and robustness of medical image segmentation and is efficient in terms of computation. The use of bag-of-activation functions offers a flexible approach to augmenting neural network efficacy, tackling intricate visual data issues in healthcare, and perhaps improved patient outcomes via more accurate segmentation masks. By adaptively integrating various activation functions, BoA improves the versatility and robustness of neural networks in diverse ML applications.

## References

- [1] Walid Al-Dhabyani, Mohammed Gomaa, Hussien Khaled, and Aly Fahmy. Dataset of breast ultrasound images. *Data in Brief*, 28:104863, 2020. 2, 6, 7
- [2] Simon Andermatt, Simon Pezold, and Philippe Cattin. Multi-dimensional gated recurrent units for the segmentation of biomedical 3d-data. *Deep Learning and Data Labeling for Medical Applications*, pages 142–151, 2016. 2
- [3] Hao Chen, Xin Qi, Lequan Yu, and Pheng-Ann Heng. Cascaded convolutional neural networks for automatic detection of thyroid nodules in ultrasound images. *Medical Physics*, 46(3):1244–1257, 2019. 3
- [4] Haojie Chen, Xin Lin, Yining Hu, Xiaoqian Yang, Haibin Guan, Yisheng Zhu, Baiying Chen, and Yefeng Zheng. Aa-net: Adaptive attention u-net for breast lesion segmentation in ultrasound images. *IEEE Transactions on Medical Imaging*, 2023. 3
- [5] Jieneng Chen, Yongyi Lu, Qihang Yu, Xiangde Luo, Ehsan Adeli, Yan Wang, Le Lu, Alan L Yuille, and Yuyin Zhou. Transunet: Transformers make strong encoders for medical image segmentation. *arXiv Preprint arXiv:2102.04306*, 2021. 1, 2
- [6] Charles Church, Icy Wong, and Yi Zhang. Deep learning for automated segmentation of medical images: A systematic review. *Journal of Medical Systems*, 43(6):127, 2019. 1
- [7] Alexey Dosovitskiy, Lucas Beyer, Alexander Kolesnikov, Dirk Weissenborn, Xiaohua Zhai, Thomas Unterthiner, Mostafa Dehghani, Matthias Minderer, Georg Heigold, Sylvain Gelly, et al. An image is worth 16x16 words: Transformers for image recognition at scale. *arXiv Preprint arXiv:2010.11929*, 2020. 1
- [8] Alexey Dosovitskiy, Lucas Beyer, Alexander Kolesnikov, Dirk Weissenborn, Xiaohua Zhai, Thomas Unterthiner, Mostafa Dehghani, Matthias Minderer, Georg Heigold, Sylvain Gelly, et al. An image is worth 16x16 words: Transformers for image recognition at scale. *arXiv preprint arXiv:2010.11929*, 2021. 2
- [9] Albert Gu, Tri Dao, Stefano Ermon, Atri Rudra, and Christopher Ré. Mamba: Linear-time sequence modeling with selective state spaces. *arXiv Preprint arXiv:2312.00752*, 2023. 1, 2, 3
- [10] Zaiwang Gu, Jun Cheng, Huazhu Fu, Kang Zhou, Huaying Hao, Yitian Zhao, Tianyang Zhang, Shenghua Gao, and Jiang Liu. Ce-net: Context encoder network for 2d medical image segmentation. *IEEE transactions on medical imaging*, 38(10):2281–2292, 2019. 2
- [11] Jun Han and Claudio Moraga. The influence of the sigmoid function parameters on the speed of backpropagation learning. *International Workshop on Artificial Neural Networks*, pages 195–201, 1995. 7
- [12] Guang-Bin Huang, Li-Ming Zhao, and Qing-Yu Song. Kolmogorov-arnold network for nonlinear function approxi-



- mation. *IEEE transactions on neural networks and learning systems*, 26(7):1345–1359, 2014. 2, 3
- [13] Huimin Huang, Lanfen Lin, Ruofeng Tong, Hongjie Hu, Qiaowei Zhang, Yutaro Iwamoto, Xianhua Han, Yen-Wei Chen, and Jian Wu. Unet 3+: A full-scale connected unet for medical image segmentation. *arXiv preprint arXiv:2004.08790*, 2020. 1
- [14] Debesh Jha, Pia H Smedsrud, Michael A Riegler, Pål Halvorsen, Thomas de Lange, Dag Johansen, and Håvard D Johansen. Kvasir-seg: A segmented polyp dataset. In *Proceedings of the International Conference on Multimedia Modeling*, pages 451–462. Springer, 2020. 2, 6, 7
- [15] Konstantinos Kamnitsas, Christian Ledig, Virginia FJ Newcombe, Joanna P Simpson, Andrew D Kane, David K Menon, Daniel Rueckert, and Ben Glocker. Efficient multi-scale 3d cnn with fully connected crf for accurate brain lesion segmentation. *Medical Image Analysis*, 36:61–78, 2017. 2
- [16] Jihane Kevric, Duygu Kocak, and Ali Çelik. Deep learning for medical image segmentation: A survey. *International Journal of Imaging Systems and Technology*, 32(2):295–308, 2022. 1
- [17] Yann LeCun, Léon Bottou, Genevieve B Orr, and Klaus-Robert Müller. Efficient backprop. *Neural networks: Tricks of the trade*, pages 9–50, 1998. 7
- [18] Chenxin Li, Xinyu Liu, Wuyang Li, Cheng Wang, Hengyu Liu, Yifan Liu, Zhen Chen, and Yixuan Yuan. U-kan makes strong backbone for medical image segmentation and generation. *arXiv Preprint arXiv:2406.02918*, 2024. 2, 3, 4, 5, 6, 7
- [19] Xiang Li, Hao Chen, Xin Qi, Qi Dou, Chi-Wing Fu, and Pheng-Ann Heng. U2-mnet: A novel medical image segmentation network based on u-net and u-net++. *IEEE Access*, 8:185122–185134, 2020. 3
- [20] Yue Liu, Yancheng Xie, Jiacheng Shi, Zeren Huang, Yunzhi Liu, Zhiwei Ye, Zhenwei Niu, Lewei Cao, Feng Xue, Shangling Wang, et al. Vmamba: Visual state space model. *arXiv Preprint arXiv:2401.10166*, 2024. 2, 3
- [21] Yunchao Liu, Weixuan Yang, Yao Zhang, Haoran Wang, Andrew F Laine, and Jianqing Fan. Rolling-unet: Enhancing u-net architecture with rolling convolution for medical image segmentation. *arXiv preprint arXiv:2401.01575*, 2024. 6, 7
- [22] Ziming Liu, Albert Gu, Tri Dao, Stefano Ermon, and Christopher Ré. Kan: Kolmogorov-arnold networks. *arXiv Preprint arXiv:2404.19756*, 2024. 2
- [23] Yunguan Lu, Song Guo, Chen Chen, Mina Amiri, Jianfei Gu, and Chengliang Tao. U-mamba: Enhancing long-range dependency for biomedical image segmentation. *arXiv Preprint arXiv:2401.04722*, 2024. 1
- [24] Jun Ma, Yao Li, and Chaowei Wang. U-mamba: Enhancing long-range dependency for biomedical image segmentation. *arXiv preprint arXiv:2401.04722*, 2024. 6, 7
- [25] Vinod Nair and Geoffrey E Hinton. Rectified linear units improve restricted boltzmann machines. *Proceedings of the 27th International Conference on Machine Learning*, pages 807–814, 2010. 7
- [26] Narinder Singh Punn and Sonali Agarwal. Attention-guided u-net with cross-layer feature fusion for breast tumor segmentation in ultrasound images. *Biomedical Signal Processing and Control*, 72:103316, 2022. 3
- [27] Olaf Ronneberger, Philipp Fischer, and Thomas Brox. U-net: Convolutional networks for biomedical image segmentation. In *MICCAI 2015*, pages 234–241. Springer, 2015. 1, 2, 6, 7
- [28] Yuxin Tang, Yinan Tang, Jing Xiao, and Ronald M Summers. Fpnn: Feature pyramid non-local network for breast cancer segmentation. *arXiv Preprint arXiv:1810.12431*, 2018. 3
- [29] Jeya Maria Jose Valanarasu, Poojan Oza, Ilker Hacihaliloglu, and Vishal M Patel. Kiu-net: Towards accurate segmentation of biomedical images using over-complete representations. *Medical Image Analysis*, 68:101743, 2021. 2, 6, 7
- [30] Jeya Maria Jose Valanarasu, Poojan Oza, Ilker Hacihaliloglu, and Vishal M Patel. Medical transformer: Gated axial-attention for medical image segmentation. In *Proceedings of MICCAI 2021*, pages 36–46. Springer, 2021. 2, 6, 7
- [31] Ashish Vaswani, Noam Shazeer, Niki Parmar, Jakob Uszkoreit, Llion Jones, Aidan N Gomez, Łukasz Kaiser, and Illia Polosukhin. Attention is all you need. In *arXiv Preprint*, pages 5998–6008, 2017. 2
- [32] Liang Wang, Siyuan Lu, Jianwei Yang, Liang-Chieh Li, and Thomas S Huang. Vision mamba: Efficient visual representation learning with bidirectional state space model. *arXiv Preprint arXiv:2401.09417*, 2024. 1
- [33] Zhaochen Wang, Yuhao Xiao, Xizhou Zhu, Yu Qiao, and Jifeng Dai. Segmamba: Long-range sequential modeling mamba for 3d medical image segmentation. *arXiv Preprint arXiv:2401.13560*, 2024. 1
- [34] Sanghyun Woo, Jongchan Park, Joon-Young Lee, and In So Kweon. Cbam: Convolutional block attention module. In *ECCV*, pages 3–19. Springer, 2018. 2, 3
- [35] Wei Zhang, Jin Liu, and Xia Wang. Medical image segmentation for robotic surgery: A review. *Medical Image Analysis*, 70:101956, 2021. 1
- [36] Zongwei Zhou, Md Mahfuzur Rahman Siddiquee, Nima Tajbakhsh, and Jianming Liang. Unet++: A nested u-net architecture for medical image segmentation. *Deep Learning in Medical Image Analysis and Multimodal Learning for Clinical Decision Support*, pages 3–11, 2018. 1, 2
- [37] Qianqian Zhu, Bo Du, and Pingkun Yan. Su-net: A novel self-attention u-net for breast cancer segmentation in ultrasound images. *IEEE Transactions on Medical Imaging*, 40(9):2353–2364, 2021. 3